Study of the normalized transverse momentum distribution of *W* bosons produced in *pp̄* collisions at $\sqrt{s} = 1.96$ TeV

V. M. Abazov,[31] B. Abbott,[67] B. S. Acharya,[25] M. Adams,[46] T. Adams,[44] J. P. Agnew,[41] G. D. Alexeev,[31] G. Alkhazov,[35] A. Alton,[56,b] A. Askew,[44] S. Atkins,[54] K. Augsten,[7] V. Aushev,[38] Y. Aushev,[38] C. Avila,[5] F. Badaud,[10] L. Bagby,[45] B. Baldin,[45] D. V. Bandurin,[74] S. Banerjee,[25] E. Barberis,[55] P. Baringer,[53] J. F. Bartlett,[45] U. Bassler,[15] V. Bazterra,[46] A. Bean,[53] M. Begalli,[2] L. Bellantoni,[45] S. B. Beri,[23] G. Bernardi,[14] R. Bernhard,[19] I. Bertram,[39] M. Besançon,[15] R. Beuselinck,[40] P. C. Bhat,[45] S. Bhatia,[58] V. Bhatnagar,[23] G. Blazey,[47] S. Blessing,[44] K. Bloom,[59] A. Boehnlein,[45] D. Boline,[64] E. E. Boos,[33] G. Borissov,[39] M. Borysova,[38,l] A. Brandt,[71] O. Brandt,[20] M. Brochmann,[75] R. Brock,[57] A. Bross,[45] D. Brown,[14] X. B. Bu,[45] M. Buehler,[45] V. Buescher,[21] V. Bunichev,[33] S. Burdin,[39,c] C. P. Buszello,[37] E. Camacho-Pérez,[28] B. C. K. Casey,[45] H. Castilla-Valdez,[28] S. Caughron,[57] S. Chakrabarti,[64] K. M. Chan,[51] A. Chandra,[73] E. Chapon,[15] G. Chen,[53] S. W. Cho,[27] S. Choi,[27] B. Choudhary,[24] S. Cihangir,[45,a] D. Claes,[59] J. Clutter,[53] M. Cooke,[45,k] W. E. Cooper,[45] M. Corcoran,[73,a] F. Couderc,[15] M.-C. Cousinou,[12] J. Cuth,[21] D. Cutts,[70] A. Das,[72] G. Davies,[40] S. J. de Jong,[29,30] E. De La Cruz-Burelo,[28] F. Déliot,[15] R. Demina,[63] D. Denisov,[65] S. P. Denisov,[34] S. Desai,[45] C. Deterre,[41,d] K. DeVaughan,[59] H. T. Diehl,[45] M. Diesburg,[45] P. F. Ding,[41] A. Dominguez,[59] A. Drutskoy,[32,q] A. Dubey,[24] L. V. Dudko,[33] A. Duperrin,[12] S. Dutt,[23] M. Eads,[47] D. Edmunds,[57] J. Ellison,[43] V. D. Elvira,[45] Y. Enari,[14] H. Evans,[49] A. Evdokimov,[46] V. N. Evdokimov,[34] A. Fauré,[15] L. Feng,[47] T. Ferbel,[63] F. Fiedler,[21] F. Filthaut,[29,30] W. Fisher,[57] H. E. Fisk,[45] M. Fortner,[47] H. Fox,[39] J. Franc,[7] S. Fuess,[45] Y. Fu,[4] P. H. Garbincius,[45] A. Garcia-Bellido,[63] J. A. García-González,[28] V. Gavrilov,[32] W. Geng,[12,57] C. E. Gerber,[46] Y. Gershtein,[60] G. Ginther,[45] O. Gogota,[38] G. Golovanov,[31] P. D. Grannis,[64] S. Greder,[16] H. Greenlee,[45] G. Grenier,[17] Ph. Gris,[10] J.-F. Grivaz,[13] A. Grohsjean,[15,d] S. Grünendahl,[45] M. W. Grünewald,[26] T. Guillemin,[13] G. Gutierrez,[45] P. Gutierrez,[67] J. Haley,[68] L. Han,[4] K. Harder,[41] A. Harel,[63] J. M. Hauptman,[52] J. Hays,[40] T. Head,[41] T. Hebbeker,[18] D. Hedin,[47] H. Hegab,[68] A. P. Heinson,[43] U. Heintz,[70] C. Hensel,[1] I. Heredia-De La Cruz,[28,e] K. Herner,[45] G. Hesketh,[41,g] M. D. Hildreth,[51] R. Hirosky,[74] T. Hoang,[44] J. D. Hobbs,[64] B. Hoeneisen,[9] J. Hogan,[73] M. Hohlfeld,[21] J. L. Holzbauer,[58] I. Howley,[71] Z. Hubacek,[7,15] V. Hynek,[7] I. Iashvili,[62] Y. Ilchenko,[72] R. Illingworth,[45] A. S. Ito,[45] S. Jabeen,[45,m] M. Jaffré,[13] A. Jayasinghe,[67] M. S. Jeong,[27] R. Jesik,[40] P. Jiang,[4,a] K. Johns,[42] E. Johnson,[57] M. Johnson,[45] A. Jonckheere,[45] P. Jonsson,[40] J. Joshi,[43] A. W. Jung,[45,o] A. Juste,[36] E. Kajfasz,[12] D. Karmanov,[33] I. Katsanos,[59] M. Kaur,[23] R. Kehoe,[72] S. Kermiche,[12] N. Khalatyan,[45] A. Khanov,[68] A. Kharchilava,[62] Y. N. Kharzheev,[31] I. Kiselevich,[32] J. M. Kohli,[23] A. V. Kozelov,[34] J. Kraus,[58] A. Kumar,[62] A. Kupco,[8] T. Kurča,[17] V. A. Kuzmin,[33] S. Lammers,[49] P. Lebrun,[17] H. S. Lee,[27] S. W. Lee,[52] W. M. Lee,[45,a] X. Lei,[42] J. Lellouch,[14] D. Li,[14] H. Li,[74] L. Li,[43] Q. Z. Li,[45] J. K. Lim,[27] D. Lincoln,[45] J. Linnemann,[57] V. V. Lipaev,[34,a] R. Lipton,[45] H. Liu,[72] Y. Liu,[4] A. Lobodenko,[35] M. Lokajicek,[8] R. Lopes de Sa,[45] R. Luna-Garcia,[28,h] A. L. Lyon,[45] A. K. A. Maciel,[1] R. Madar,[19] R. Magaña-Villalba,[28] S. Malik,[59] V. L. Malyshev,[31] J. Mansour,[20] J. Martínez-Ortega,[28] R. McCarthy,[64] C. L. McGivern,[41] M. M. Meijer,[29,30] A. Melnitchouk,[45] D. Menezes,[47] P. G. Mercadante,[3] M. Merkin,[33] A. Meyer,[18] J. Meyer,[20,j] F. Miconi,[16] N. K. Mondal,[25] M. Mulhearn,[74] E. Nagy,[12] M. Narain,[70] R. Nayyar,[42] H. A. Neal,[56,a] J. P. Negret,[5] P. Neustroev,[35] H. T. Nguyen,[74] T. Nunnemann,[22] J. Orduna,[70] N. Osman,[12] A. Pal,[71] N. Parashar,[50] V. Parihar,[70] S. K. Park,[27] R. Partridge,[70,f] N. Parua,[49] A. Patwa,[65,k] B. Penning,[40] M. Perfilov,[33] Y. Peters,[41] K. Petridis,[41] G. Petrillo,[63] P. Pétroff,[13] M.-A. Pleier,[65] V. M. Podstavkov,[45] A. V. Popov,[34] M. Prewitt,[73] D. Price,[41] N. Prokopenko,[34] J. Qian,[56] A. Quadt,[20] B. Quinn,[58] P. N. Ratoff,[39] I. Razumov,[34] I. Ripp-Baudot,[16] F. Rizatdinova,[68] M. Rominsky,[45] A. Ross,[39] C. Royon,[8] P. Rubinov,[45] R. Ruchti,[51] G. Sajot,[11] A. Sánchez-Hernández,[28] M. P. Sanders,[22] A. S. Santos,[1,i] G. Savage,[45] M. Savitskyi,[38] L. Sawyer,[54] T. Scanlon,[40] R. D. Schamberger,[64] Y. Scheglov,[35,a] H. Schellman,[69,48] M. Schott,[21] C. Schwanenberger,[41,d] R. Schwienhorst,[57] J. Sekaric,[53] H. Severini,[67] E. Shabalina,[20] V. Shary,[15] S. Shaw,[41] A. A. Shchukin,[34] O. Shkola,[38] V. Simak,[7,a] P. Skubic,[67] P. Slattery,[63] G. R. Snow,[59,a] J. Snow,[66] S. Snyder,[65] S. Söldner-Rembold,[41] L. Sonnenschein,[18] K. Soustruznik,[6] J. Stark,[11] N. Stefaniuk,[38] D. A. Stoyanova,[34] M. Strauss,[67] L. Suter,[41] P. Svoisky,[74] M. Titov,[15] V. V. Tokmenin,[31] Y.-T. Tsai,[63] D. Tsybychev,[64] B. Tuchming,[15] C. Tully,[61] L. Uvarov,[35] S. Uvarov,[35] S. Uzunyan,[47] R. Van Kooten,[49] W. M. van Leeuwen,[29] N. Varelas,[46] E. W. Varnes,[42] I. A. Vasilyev,[34] A. Y. Verkheev,[31] L. S. Vertogradov,[31] M. Verzocchi,[45] M. Vesterinen,[41] D. Vilanova,[15] P. Vokac,[7] H. D. Wahl,[44] C. Wang,[4] M. H. L. S. Wang,[45] J. Warchol,[51,a] G. Watts,[75] M. Wayne,[51] J. Weichert,[21] L. Welty-Rieger,[48] M. R. J. Williams,[49,n] G. W. Wilson,[53] M. Wobisch,[54] D. R. Wood,[55] T. R. Wyatt,[41] Y. Xie,[45] R. Yamada,[45] S. Yang,[4] T. Yasuda,[45] Y. A. Yatsunenko,[31] W. Ye,[64] Z. Ye,[45] H. Yin,[45] K. Yip,[65] S. W. Youn,[45] J. M. Yu,[56] J. Zennamo,[62] T. G. Zhao,[41] B. Zhou,[56] J. Zhu,[56] M. Zielinski,[63] D. Zieminska,[49] and L. Zivkovic[14,p]

(The D0 Collaboration)

[1]*LAFEX, Centro Brasileiro de Pesquisas Físicas, Rio de Janeiro, RJ 22290, Brazil*
[2]*Universidade do Estado do Rio de Janeiro, Rio de Janeiro, RJ 20550, Brazil*
[3]*Universidade Federal do ABC, Santo André, SP 09210, Brazil*
[4]*University of Science and Technology of China, Hefei 230026, People's Republic of China*
[5]*Universidad de los Andes, Bogotá, 111711, Colombia*
[6]*Charles University, Faculty of Mathematics and Physics, Center for Particle Physics,*
116 36 Prague 1, Czech Republic
[7]*Czech Technical University in Prague, 116 36 Prague 6, Czech Republic*
[8]*Institute of Physics, Academy of Sciences of the Czech Republic, 182 21 Prague, Czech Republic*
[9]*Universidad San Francisco de Quito, Quito 170157, Ecuador*
[10]*LPC, Université Blaise Pascal, CNRS/IN2P3, Clermont, F-63178 Aubière Cedex, France*
[11]*LPSC, Université Joseph Fourier Grenoble 1, CNRS/IN2P3,*
Institut National Polytechnique de Grenoble, F-38026 Grenoble Cedex, France
[12]*CPPM, Aix-Marseille Université, CNRS/IN2P3, F-13288 Marseille Cedex 09, France*
[13]*LAL, Univ. Paris-Sud, CNRS/IN2P3, Université Paris-Saclay, F-91898 Orsay Cedex, France*
[14]*LPNHE, Universités Paris VI and VII, CNRS/IN2P3, F-75005 Paris, France*
[15]*IRFU, CEA, Université Paris-Saclay, F-91191 Gif-Sur-Yvette, France*
[16]*IPHC, Université de Strasbourg, CNRS/IN2P3, F-67037 Strasbourg, France*
[17]*IPNL, Université Lyon 1, CNRS/IN2P3, F-69622 Villeurbanne Cedex, France and Université de Lyon,*
F-69361 Lyon CEDEX 07, France
[18]*III. Physikalisches Institut A, RWTH Aachen University, 52056 Aachen, Germany*
[19]*Physikalisches Institut, Universität Freiburg, 79085 Freiburg, Germany*
[20]*II. Physikalisches Institut, Georg-August-Universität Göttingen, 37073 Göttingen, Germany*
[21]*Institut für Physik, Universität Mainz, 55099 Mainz, Germany*
[22]*Ludwig-Maximilians-Universität München, 80539 München, Germany*
[23]*Panjab University, Chandigarh 160014, India*
[24]*Delhi University, Delhi-110 007, India*
[25]*Tata Institute of Fundamental Research, Mumbai-400 005, India*
[26]*University College Dublin, Dublin 4, Ireland*
[27]*Korea Detector Laboratory, Korea University, Seoul 02841, Korea*
[28]*CINVESTAV, Mexico City 07360, Mexico*
[29]*Nikhef, Science Park, 1098 XG Amsterdam, Netherlands*
[30]*Radboud University Nijmegen, 6525 AJ Nijmegen, Netherlands*
[31]*Joint Institute for Nuclear Research, Dubna 141980, Russia*
[32]*Institute for Theoretical and Experimental Physics, Moscow 117259, Russia*
[33]*Moscow State University, Moscow 119991, Russia*
[34]*Institute for High Energy Physics, Protvino, Moscow Region 142281, Russia*
[35]*Petersburg Nuclear Physics Institute, St. Petersburg 188300, Russia*
[36]*Institució Catalana de Recerca i Estudis Avançats (ICREA) and Institut de Física d'Altes Energies*
(IFAE), 08193 Bellaterra (Barcelona), Spain
[37]*Uppsala University, 751 05 Uppsala, Sweden*
[38]*Taras Shevchenko National University of Kyiv, Kiev 01601, Ukraine*
[39]*Lancaster University, Lancaster LA1 4YB, United Kingdom*
[40]*Imperial College London, London SW7 2AZ, United Kingdom*
[41]*The University of Manchester, Manchester M13 9PL, United Kingdom*
[42]*University of Arizona, Tucson, Arizona 85721, USA*
[43]*University of California Riverside, Riverside, California 92521, USA*
[44]*Florida State University, Tallahassee, Florida 32306, USA*
[45]*Fermi National Accelerator Laboratory, Batavia, Illinois 60510, USA*
[46]*University of Illinois at Chicago, Chicago, Illinois 60607, USA*
[47]*Northern Illinois University, DeKalb, Illinois 60115, USA*
[48]*Northwestern University, Evanston, Illinois 60208, USA*
[49]*Indiana University, Bloomington, Indiana 47405, USA*
[50]*Purdue University Calumet, Hammond, Indiana 46323, USA*
[51]*University of Notre Dame, Notre Dame, Indiana 46556, USA*
[52]*Iowa State University, Ames, Iowa 50011, USA*
[53]*University of Kansas, Lawrence, Kansas 66045, USA*
[54]*Louisiana Tech University, Ruston, Louisiana 71272, USA*
[55]*Northeastern University, Boston, Massachusetts 02115, USA*
[56]*University of Michigan, Ann Arbor, Michigan 48109, USA*

[57]*Michigan State University, East Lansing, Michigan 48824, USA*
[58]*University of Mississippi, University, Mississippi 38677, USA*
[59]*University of Nebraska, Lincoln, Nebraska 68588, USA*
[60]*Rutgers University, Piscataway, New Jersey 08855, USA*
[61]*Princeton University, Princeton, New Jersey 08544, USA*
[62]*State University of New York, Buffalo, New York 14260, USA*
[63]*University of Rochester, Rochester, New York 14627, USA*
[64]*State University of New York, Stony Brook, New York 11794, USA*
[65]*Brookhaven National Laboratory, Upton, New York 11973, USA*
[66]*Langston University, Langston, Oklahoma 73050, USA*
[67]*University of Oklahoma, Norman, Oklahoma 73019, USA*
[68]*Oklahoma State University, Stillwater, Oklahoma 74078, USA*
[69]*Oregon State University, Corvallis, Oregon 97331, USA*
[70]*Brown University, Providence, Rhode Island 02912, USA*
[71]*University of Texas, Arlington, Texas 76019, USA*
[72]*Southern Methodist University, Dallas, Texas 75275, USA*
[73]*Rice University, Houston, Texas 77005, USA*
[74]*University of Virginia, Charlottesville, Virginia 22904, USA*
[75]*University of Washington, Seattle, Washington, D.C. 98195, USA*

We present a study of the normalized transverse momentum distribution of W bosons produced in $p\bar{p}$ collisions, using data corresponding to an integrated luminosity of 4.35 fb^{-1} collected with the D0 detector at the Fermilab Tevatron collider at $\sqrt{s} = 1.96$ TeV. The measurement focuses on the transverse momentum region below 15 GeV, which is of special interest for electroweak precision measurements; it relies on the same detector calibration methods which were used for the precision measurement of the W boson mass. The measured distribution is compared to different QCD predictions and a procedure is given to allow the comparison of any further theoretical models to the D0 data.

I. INTRODUCTION

The production of $V = (W/Z)$ bosons in hadron collisions is described by perturbative quantum chromodynamics (QCD). At leading order, QCD predicts no transverse momentum of the W or Z boson (p_T^V) with respect to the beam direction [1]. However, this changes when including higher order corrections, so that significant p_T^V can arise from the emission of partons in the initial state as well as from the intrinsic transverse momentum of the initial-state partons in the

[a]Deceased.
[b]With visitor from Augustana College, Sioux Falls, South Dakota 57197, USA.
[c]With visitor from The University of Liverpool, Liverpool L69 3BX, United Kingdom.
[d]With visitor from Deutshes Elektronen-Synchrotron (DESY), Notkestrasse 85, Germany.
[e]With visitor from CONACyT, M-03940 Mexico City, Mexico.
[f]With visitor from SLAC, Menlo Park, California 94025, USA.
[g]With visitor from University College London, London WC1E 6BT, United Kingdom.
[h]With visitor from Centro de Investigacion en Computacion—IPN, CP 07738 Mexico City, Mexico.
[i]With visitor from Universidade Estadual Paulista, São Paulo, SP 01140, Brazil.
[j]With visitor from Karlsruher Institut für Technologie (KIT)—Steinbuch Centre for Computing (SCC), D-76128 Karlsruhe, Germany.
[k]With visitor from Office of Science, U.S. Department of Energy, Washington, D.C. 20585, USA.
[l]With visitor from Kiev Institute for Nuclear Research (KINR), Kyiv 03680, Ukraine.
[m]With visitor from University of Maryland, College Park, Maryland 20742, USA.
[n]With visitor from European Orgnaization for Nuclear Research (CERN), CH-1211 Geneva, Switzerland.
[o]With visitor from Purdue University, West Lafayette, Indiana 47907, USA.
[p]With visitor from Institute of Physics, Belgrade, Belgrade, Serbia.
[q]With visitor from P.N. Lebedev Physical Institute of the Russian Academy of Sciences, 119991 Moscow, Russia.

proton. The p_T^V spectrum at low transverse momentum can be described using soft-gluon resummation [2–7], parton shower approaches [8–10], and nonperturbative calculations [11,12] to account for the intrinsic transverse momentum of partons. In the nonperturbative approach [11,12], a function is introduced as a form factor in order to make the QCD calculation convergent when $p_T^V \rightarrow 0^+$. The values of the parameters in the nonperturbative function can only be extracted from the measurement of the p_T^V distribution. Knowledge of the p_T^V spectrum is not only important for testing perturbative QCD predictions and constraining models of nonperturbative approaches, but also for the measurement of electroweak parameters such as the W boson mass. In the latter case, it is especially important to model the p_T^W spectrum correctly in the low p_T region.

The transverse momentum spectrum of the Z boson has been measured to high precision at various energies, both at the Tevatron [13–16] and the LHC [17–22]. This precision is enabled by the fact that leptonically-decaying Z bosons can be easily reconstructed from the two charged leptons in the final state. The situation is different for the W boson as the neutrino escapes detection and hadronic decays have large backgrounds. The p_T^W must therefore be estimated from the reconstructed hadronic recoil of the event. The hadronic recoil is only an approximation of $p_T(W)$ as it is significantly affected by the number of simultaneous hadron collisions in the recorded event and by the nonlinear energy response of the detector for low energy hadrons.

The p_T^W distribution was previously measured at the Tevatron at $\sqrt{s} = 1.8$ TeV [23,24], and at the LHC at $\sqrt{s} = 7$ and 8 TeV [22,25]. This study is the first p_T^W analysis at $\sqrt{s} = 1.96$ TeV. In this paper, we analyze data corresponding to an integrated luminosity of 4.35 fb^{-1} collected by the D0 detector at the Fermilab Tevatron collider. These data were also used for the W boson mass measurement in Ref. [26]. This study concentrates on the low p_T^W region and resolves the peak near $p_T^W = 4$ GeV, unlike the LHC measurements of Refs. [22,25] where the sizes of the first bin are 8 GeV and 7.5 GeV, respectively. In addition, we study the transverse momentum of W bosons in the case where the production is dominated by valence quarks, unlike the situation at the LHC which involves sea quarks. Typical Bjorken x-values for W boson production at the Tevatron (LHC) are 0.05 (0.015) [1].

This paper is structured as follows: after a short description of the D0 detector, the event selection, the calibration procedure, and the basic comparison plots between data and simulation are presented. This is followed by a description of the analysis procedure. After a discussion of the systematic uncertainties, the final results are presented and compared with several models of W boson production and parton distribution functions. Finally, a fast folding procedure is introduced in the Appendix, which can be used to compare our result

to other theoretical predictions while properly accounting for the detector response.

II. THE D0 DETECTOR

The D0 detector [27] comprises a central tracking system, a calorimeter, and a muon system. The analysis uses a cylindrical coordinate system with the z axis along the beam axis in the proton direction. Angles θ and ϕ are the polar and azimuthal angles, respectively. Pseudorapidity is defined as $\eta = -\ln[\tan(\theta/2)]$ where θ is measured with respect to the interaction vertex. We define η_{det} as the pseudorapidity measured with respect to the center of the detector. The central tracking system consists of a silicon microstrip tracker (SMT) and a scintillating fiber tracker, both located within a 1.9 T superconducting solenoid magnet and optimized for tracking and vertexing for $|\eta_{\text{det}}| < 2.5$. Outside the solenoid, liquid argon and uranium calorimeters provide energy measurement, with a central calorimeter (CC) that covers $|\eta_{\text{det}}| \leq 1.05$, and two end calorimeters (EC) that extend coverage to $|\eta_{\text{det}}| < 4.2$. The muon system located outside the calorimeter consists of drift tubes and scintillators before and after 1.8 T iron toroid magnets and provides coverage for $|\eta_{\text{det}}| < 2.0$. Muons are identified and their momenta are measured using information from both the tracking system and the muon system. The solenoid and toroid polarities are reversed every two weeks on average during the periods of data-taking.

III. EVENT SAMPLES AND EVENT SELECTION

The present analysis builds on the techniques developed in Refs. [26] and [28] for the measurement of the W boson mass. Events are selected using a trigger requiring at least one electromagnetic (EM) cluster found in the CC, with the transverse energy threshold varying from 25 to 27 GeV depending on run conditions. The offline selection of candidate W boson events is the same as used in Ref. [26]. We require candidate electrons to be matched in (η, ϕ) space to a track including at least one SMT hit. The electron three-momentum vector magnitude is defined by the cluster energy, and the direction is defined by the track.

We require the presence of an electron with $p_T^e > 25$ GeV and $|\eta^e| < 1.05$ that passes shower shape and isolation requirements. Here p_T^e is the magnitude of the transverse momentum of the electron, $\vec{p}_T^e$, and η^e is the pseudorapidity of the electron. The event must satisfy $\not{E}_T > 25$ GeV, $u_T < 15$ GeV, and $50 < m_T < 200$ GeV. Here, the hadronic recoil $\vec{u}_T$ is the vector sum of the transverse component of the energies measured in calorimeter cells excluding those associated with the reconstructed electron, and u_T is its magnitude. The relation $\vec{\not{E}}_T = -(\vec{p}_T^e + \vec{u}_T)$ defines the missing transverse energy approximating the transverse momentum of the neutrino,

and m_T is the transverse mass defined as $m_T = \sqrt{2p_T^e \not{E}_T (1 - \cos \Delta\phi)}$, where $\Delta\phi$ is the azimuthal opening angle between $\vec{p}_T^e$ and $\vec{\not{E}}_T$. This selection yields 1 677 394 candidate $W \to e\nu$ events.

The $Z \to ee$ events were used extensively to calibrate the detector response [26,28], and they are also used in this study. These events are required to have two EM clusters satisfying the W candidate cluster requirements above, except that one of the two clusters may be reconstructed within an EC ($1.5 < |\eta| < 2.5$). The associated tracks must be of opposite curvature. The Z boson events must also have $u_T < 15$ GeV and $70 \leq m_{ee} \leq 110$ GeV, where m_{ee} is the invariant mass of the electron-positron pair.

The RESBOS [3] event generator, combined with PHOTOS [29], is used as a baseline simulation for the kinematics of W and Z boson production and decay. RESBOS is a next-to-leading order event generator including next-to-next-to-leading logarithm resummation of soft gluons [2], and PHOTOS generates up to two final state radiated photons. At low transverse momentum ($p_T^V < 10$ GeV), multiple soft gluon emissions dominate the cross section and a soft-gluon resummation formalism is used to make QCD predictions. This technique was first developed by Collins, Soper, and Sterman (CSS) [2] and is currently implemented using a parametric function introduced by Brock, Landry, Nadolsky and Yuan (BLNY) [30] based on three non-perturbative parameters g_1, g_2 and g_3. In the kinematic region of this measurement, the p_T^W distribution is insensitive to g_3, but can be used to constrain g_1 and g_2. The baseline simulation relies on the CTEQ6.6 [31] PDF set, as well as setting the nonperturbative parameters to the following values from Ref. [30]: $g_1 = 0.21$ GeV^2, $g_2 = 0.68$ GeV^2, and $g_3 = -0.60$ GeV^2.

We compare our measurement with predictions from various Monte Carlo (MC) simulations (RESBOS and PYTHIA [9]), different PDF sets (CT14HERA2NNLO [32,33], CTEQ6L1 [34], MSTW2008LO [35] and MRST LO [36]) and two nonperturbative functional forms (BLNY and the transverse momentum dependent TMD-BLNY [37]):

 (1) RESBOS (Version CP020811)+BLNY+CTEQ6.6
 (2) RESBOS (Version CP112216)+TMD-BLNY+CT14HERA2NNLO
 (3) PYTHIA 8+CT14HERA2NNLO
 (4) PYTHIA 8+ATLAS MB A2Tune [38]+CTEQ6L1
 (5) PYTHIA 8+ATLAS MB A2Tune [38]+MSTW2008LO
 (6) PYTHIA 8+ATLAS AZTune [18]+CT14HERA2NNLO
 (7) PYTHIA 8+Tune2C [39]+CTEQ6L1
 (8) PYTHIA 8+Tune2M [39]+MRST LO
 (9) PYTHIA 8+CMS UE Tune CUETP8S1-CTEQ6L1 [40]+CTEQ6L1

A fast parametrized MC simulation (PMCS), which is also used in our W boson mass measurement [26,28], is used to simulate electron identification efficiencies and the energy responses and resolutions of the electron and recoil system. The PMCS parameters are determined using a combination of GEANT3-based detailed simulation [41] and control data samples. The primary control sample used for both the electromagnetic and hadronic response tuning is $Z \to ee$ events. Events recorded in random beam crossings are overlaid on W and Z boson events in the simulation to emulate the effect of additional collisions in the same or nearby beam bunch crossings.

IV. DETECTOR RESPONSE CALIBRATION

The Z boson mass and width are used to calibrate the electromagnetic calorimeter energy response assuming a form $E^{\text{meas}} = \alpha E^{\text{true}} + \beta$, with constants α and β determined from fits to the dielectron mass spectrum and the energy and angular distributions of the two electrons. The hadronic energy in the event contains the hadronic system recoiling from the W boson, the effects of low energy products from spectator parton collisions and other beam collisions, final state radiation, and energy from the recoil particles that enters the electron selection window. The hadronic response (resolution) is calibrated using the mean (width) of the η_{imb} distribution in $Z \to ee$ events in bins of the dielectron transverse momentum (p_T^{ee}). Here, η_{imb} is defined as the projection of the sum of $\vec{p}_T^{ee}$ and $\vec{u}_T$ vectors on the axis bisecting the electron directions in the transverse plane [42]. More details can be found in Ref. [28].

V. BACKGROUNDS AND DATA/MC COMPARISONS

The background in the W boson candidate sample includes $Z \to ee$ events where one electron escapes detection, multijet events where a jet is misidentified as an electron with $\not{E}_T$ arising from instrumental effects, and $W \to \tau\nu \to e\nu\nu\nu$ events. The $Z \to ee$ and multijet backgrounds are estimated from collider data, and the $W \to \tau\nu \to e\nu\nu\nu$ background is obtained from the PMCS simulation of the process, as detailed in Ref. [28]. The fractions of these backgrounds relative to the signal are $1.08\% \pm 0.02\%$ for $Z \to ee$, $1.02\% \pm 0.06\%$ for multijet events, and $1.668\% \pm 0.004\%$ for $W \to \tau\nu \to e\nu\nu\nu$.

Several kinematic distributions of the signal predictions of PMCS together with the expected background contributions taken from Ref. [28] are compared to data for W boson candidate events in Figs. 1 and 2. The lepton transverse momentum, the lepton rapidity, the transverse mass, and the missing transverse energy shown in Fig. 1, are not directly sensitive to p_T^W and therefore probe the general consistency of the simulation. To test the hadronic recoil modeling, we show in Fig. 2 the data and MC comparisons for the components of the hadronic recoil parallel to ($u_{\parallel}$) and perpendicular to ($u_{\perp}$) the direction
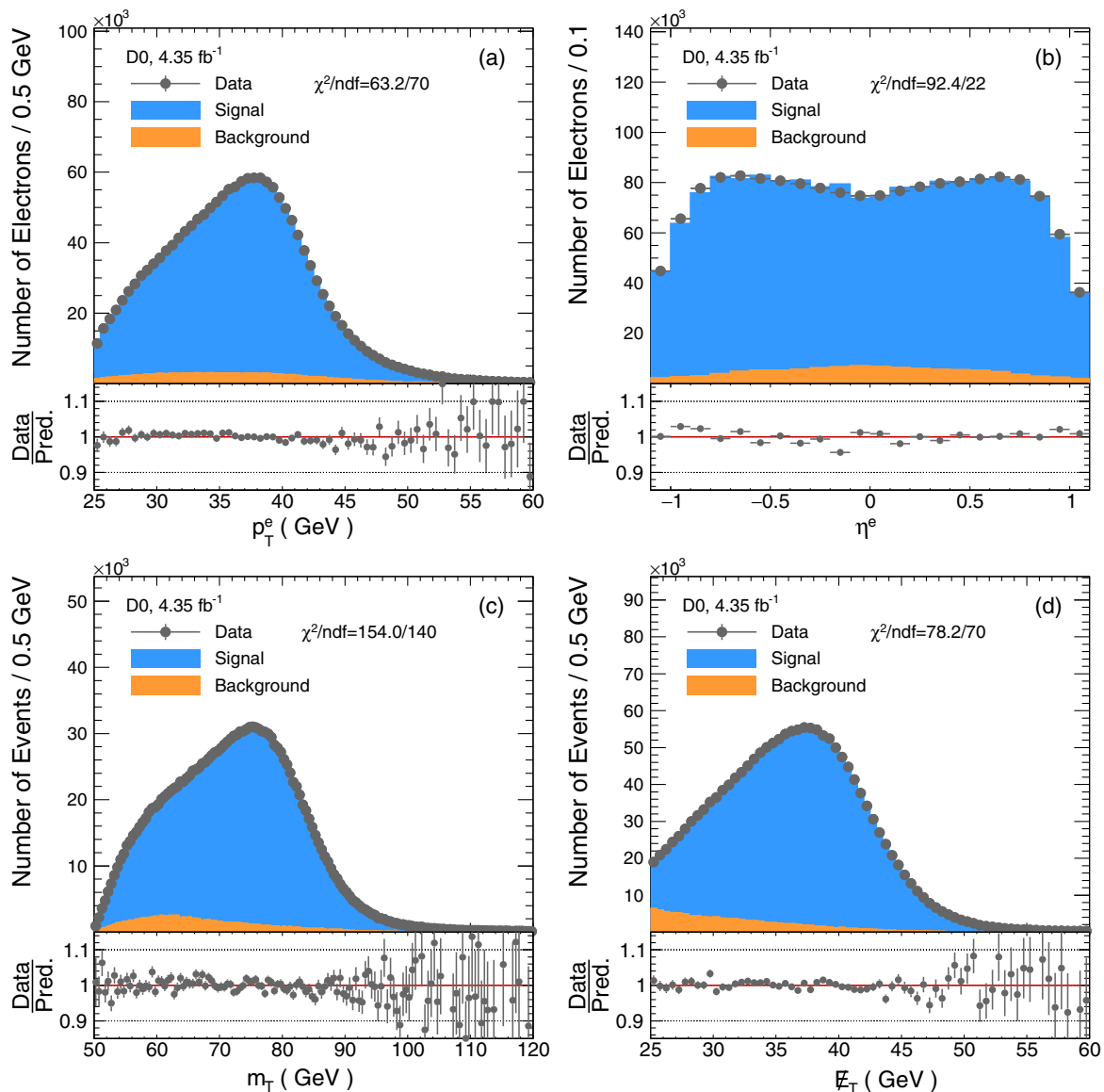
FIG. 1. Kinematic distributions for (a) p_T^e, (b) η^e, (c) m_T, (d) $\not{E}_T$. The data are compared to the PMCS plus background prediction in the upper panel, and the ratio of the data to the PMCS plus background prediction is shown in the lower panels. Only the statistical uncertainty is included.

of the electron. For all distributions in Figs. 1 and 2, the simulation is found to agree with the data.

VI. ANALYSIS STRATEGY

The comparison of several p_T^W models to data can be achieved either by comparing unfolded data directly with the predictions or by comparing predictions after accounting for detector response and resolution effects with background-subtracted data. Here folding refers to the modification of the model due to detector effects so as to compare directly to the reconstructed level data. Unfolding is the reverse transformation of the data to the particle level for comparison with the theoretical model.

The limited u_T detector resolution implies a large sensitivity to statistical fluctuations when unfolding, which have to be mitigated by a regularization scheme that increases the possible bias and thus the overall uncertainty. We therefore choose to perform the comparisons with the theory prediction at the reconstruction level.

The folding of the different theory predictions with the D0 detector response is based on the PMCS framework. In the first step, the baseline model of the W boson production is reweighted in two dimensions, p_T^W and y^W, to an alternative theory prediction to be tested. Here y^W is the rapidity of the W boson, which is highly correlated with p_T^W. In the second step, the reweighted theory
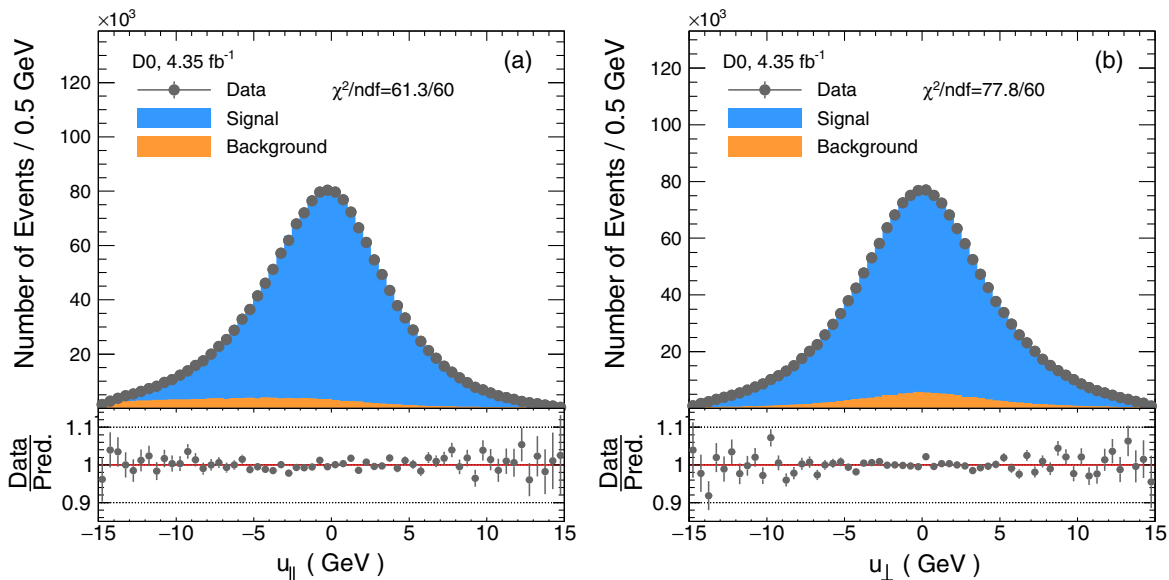
FIG. 2. Kinematic distributions for (a) $u_\parallel$, (b) $u_\perp$. The data are compared to the PMCS plus background prediction in the upper panel, and the ratio of the data to the PMCS plus background prediction is shown in the lower panels. Only the statistical uncertainty is included.

prediction is used as input for the PMCS framework, resulting in detector level distributions of all relevant observables. In the third step, the uncertainties due to limited MC statistics, the hadronic recoil calibration, the electron identification and reconstruction efficiencies, as well as the electron energy response are estimated for each theory prediction by varying all relevant detector response parameters of the PMCS framework within their uncertainties. Uncertainties due to limited MC statistics, the uncertainties due to the electron identification and reconstruction efficiencies as well as the electron energy response are found to be negligible for the u_T distribution. The hadronic recoil calibration is modeled by five calibration parameters [28]. These five parameters are divided into two groups, one containing three parameters for the response of u_T and the other containing two parameters for the resolution of u_T. Only the parameters in the same group are considered to be correlated. Given the correlation matrices of these two groups of parameters, these five parameters are transformed into another five uncorrelated parameters by a linear combination. Each component of the hadronic recoil uncertainty is estimated by varying one of the five uncorrelated parameters with its uncertainty. The combined hadronic recoil uncertainty is calculated by adding in quadrature the individual components in each u_T bin. The uncertainty from each component is considered to be bin-by-bin correlated, and the uncertainties from different components are assumed to be uncorrelated.

The uncertainties on the measured u_T distribution of the background-subtracted data are the statistical uncertainty, which is treated as bin-to-bin uncorrelated, and the uncertainty due to the background, which is significantly smaller than the statistical uncertainty. The background uncertainty is obtained by varying the overall number of events from each background contribution independently within its uncertainty, so this uncertainty should be considered to be bin-by-bin correlated. Because the uncertainties are small, the effects of these correlations are found to be negligible.

The resulting fractions of events in the u_T bins with boundaries [0,2,5,8,11,15] GeV are summarized in Table I for the background-subtracted data along with the combined statistical and systematic uncertainties.

TABLE I. The fraction of W boson events in bins of u_T for the background-subtracted data. The combined statistical and systematic uncertainties are shown.

u_T bin	0–2 GeV	2–5 GeV	5–8 GeV	8–11 GeV	11–15 GeV
Fraction of events in the u_T bin	0.1181	0.3603	0.2738	0.1515	0.0963
Total uncertainty	0.0003	0.0005	0.0005	0.0004	0.0003

FIG. 3. Comparisons of the measured and predicted u_T distributions after the detector response simulation for different MC predictions based on RESBOS. The ratios of the background-subtracted data to each theory prediction are shown in the lower panel together with the 1σ uncertainty band. The total experimental uncertainty is indicated by the hatched band; it is dominated by the uncertainty due to the hadronic recoil calibration. The points for the predictions are offset horizontally to aid with visibility.

VII. RESULTS AND COMPARISON TO THEORY

At the reconstruction level, the u_T distribution of the background-subtracted data is compared to the predictions of RESBOS and PYTHIA listed in Sec. III. The predictions are normalized to the background-subtracted data with $u_T < 15$ GeV. The data are compared to RESBOS predictions based on two different nonperturbative functions, BLNY and TMD-BLNY in Fig. 3. Figure 4 shows comparisons with PYTHIA predictions using the different tunes provided by several collaborations. All five u_T bins are considered in the χ^2 calculation. The uncertainties due to the resummation calculation of RESBOS and the tune of PYTHIA are not considered in the comparison and the χ^2 calculation, and the uncertainty due to the PDF set is negligible. Since both the data and the prediction are normalized to unity, the number of degrees of freedom is 4. The resulting χ^2/ndf values for all models and the corresponding significances in the Gaussian approximation are summarized in Table II. From this comparison, PYTHIA 8+ ATLAS MB A2Tune+CTEQ6L1 is excluded with a p-value equal to 5.84×10^{-10} and PYTHIA 8+CMS UE Tune CUETP8S1-CTEQ6L1+CTEQ6L1 is excluded with a p-value equal to 4.23×10^{-7}. All the other PYTHIA 8 predictions except the default, PYTHIA 8+CT14HERA2NNLO, are disfavored. The model based on RESBOS+BLNY agrees with the data.
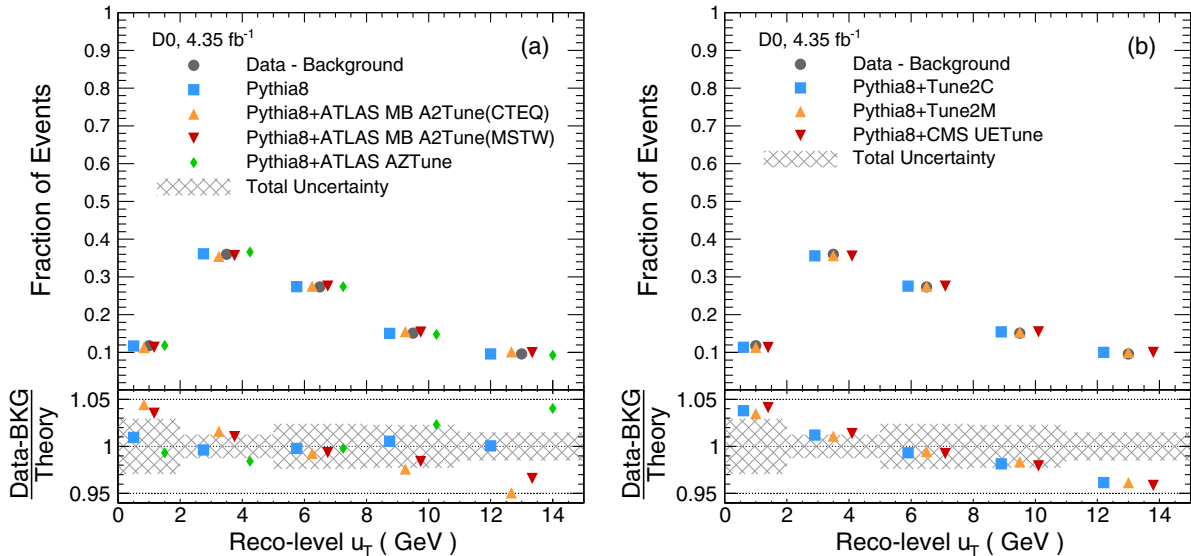
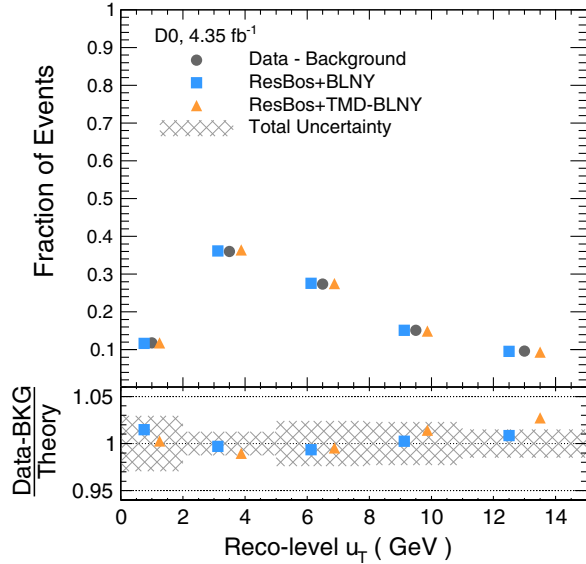
FIG. 4. Comparisons of the measured and predicted u_T distributions after the detector response simulation for different MC predictions based on PYTHIA. The ratios of the background-subtracted data to each theory prediction are shown in the lower panel together with the 1σ uncertainty band. The total experimental uncertainty is indicated by the hatched band; it is dominated by the uncertainty due to the hadronic recoil calibration. The points for the predictions are offset horizontally to aid with visibility.

TABLE II. Chi-squared per degree of freedom and the corresponding p-value for the reconstructed-level comparison. Significance is the number of standard deviations in the Gaussian approximation for the difference between each model and the background-subtracted data. Since the distributions are normalized to unity before the comparison, the number of degrees of freedom is 4.

Generator/Model	χ^2/ndf	p-value	Signif.
RESBOS (Version CP 020811)+BLNY+CTEQ6.6	0.49	7.41×10^{-1}	0.33
RESBOS (Version CP 112216)+TMD-BLNY+CT14HERA2NNLO	3.13	1.39×10^{-2}	2.46
PYTHIA 8+CT14HERA2NNLO	0.32	8.63×10^{-1}	0.17
PYTHIA 8+ATLAS MB A2Tune+CTEQ6L1	12.25	5.84×10^{-10}	6.19
PYTHIA 8+ATLAS MB A2Tune+MSTW2008LO	6.17	5.83×10^{-5}	4.02
PYTHIA 8+ATLAS AZTune+CT14HERA2NNLO	6.61	2.60×10^{-5}	4.21
PYTHIA 8+Tune2C+CTEQ6L1	7.66	3.61×10^{-6}	4.63
PYTHIA 8+Tune2M+MRSTLO	7.32	6.89×10^{-6}	4.50
PYTHIA 8+CMS UE Tune CUETP8S1-CTEQ6L1+CTEQ6L1	8.80	4.23×10^{-7}	5.06

VIII. CONCLUSION

We report a study of the normalized transverse momentum distribution of W bosons produced in $p\bar{p}$ collisions at a center of mass energy of 1.96 TeV, using 4.35 fb^{-1} of data collected by the D0 collaboration at the Fermilab Tevatron collider. The u_T distribution of the data is compared to those from several theory predictions at the reconstruction level. From these comparisons, PYTHIA 8+ ATLAS MB A2Tune+CTEQ6L1 and PYTHIA 8+CMS UE Tune CUETP8S1- CTEQ6L1+CTEQ6L1 are excluded. All the other PYTHIA 8 predictions except the default, PYTHIA 8+ CT14HERA2NNLO, are disfavored. Both models based on RESBOS give satisfactory fits to the data. The precision is limited by the uncertainty due to the hadronic recoil calibration.

In the Appendix, we describe a procedure by which theoretical models for the p_T distribution of W boson production beyond those considered in this paper can be quantitatively compared to the D0 data.

This study is the first inclusive p_T^W analysis using Tevatron Run II data. Our data are binned sufficiently finely in p_T^W to resolve the peak in the cross section, unlike the previous measurements at the LHC. In comparison to measurements by LHC experiments, which involve sea quarks, this work provides additional information for evaluating resummation calculations of transverse momentum of W bosons when the production is dominated by valence quarks.

APPENDIX: DETECTOR RESPONSE FOR FUTURE COMPARISONS

In order to compare additional model predictions to the measured data, some previous measurements [22,24,25] have been unfolded to the particle level. However, in this study, instead of providing the unfolded particle level p_T^W distribution, a fast folding procedure is introduced for two reasons: first, no new piece of information would be added by the unfolding procedure so the precision on the particle level would not be better than that on the reconstruction level. Due to the systematic uncertainty from the MC

modeling or the regularization which would be introduced by an unfolding method, the precision of the unfolded particle level distribution would be reduced. This reduction would be greater when the resolution of the distribution is worse, and it would be smaller when the bin width is enlarged. But when the bin width is too large, the rise and hence the shape of the spectrum cannot be resolved. Second, it is hard to estimate the bin-by-bin correlation of the uncertainty due to the MC modeling or the regularization properly, since the definitions of these uncertainties are often arbitrary. Therefore, the folding method provided gives a more precise and reliable means of comparison than would an unfolded result.

This fast folding procedure has to be applied on p_T^W spectra within the fiducial region defined by an electron with $p_T^e > 25$ GeV and $|\eta^e| < 1.05$, a W boson with $50 < m_T < 200$ GeV and a neutrino with $p_T^\nu > 25$ GeV. The numbers of events in p_T^W bins with boundaries [0, 2, 5, 8, 11, 15, 600] GeV are the input to this folding procedure.

In the first step, the spectrum has to be corrected for the detector efficiency in each p_T^W bin, via

$$X_i^{\text{corr}} = \mathcal{E}_i X_i.$$

Here X_i is the number of events in bin i of the p_T^W distribution within the fiducial region, $\mathcal{E}_i$ is the detector efficiency summarized in Table III and X_i^{corr} is the number of efficiency-corrected events on the particle level in bin i. Even though most of the events with $p_T^W > 100$ GeV will not satisfy $u_T < 15$ GeV after the PMCS simulation, we still chose 600 GeV as the upper edge of the last p_T^W bin. This is because the efficiency correction in the last p_T^W bin is directly related to this choice, and the upper edge of the last p_T^W bin should be kept the same as the value used when deriving those efficiency correction factors.

The second step accounts for the mapping from p_T^W to u_T using the response matrix R_{ij} via

$$N_i = \sum_{j=1}^{6} R_{ij} X_j^{\text{corr}},$$

where N_i is the resulting number of events of the reconstruction level in bin i and R_{ij} is a 5×6 matrix. The response matrix is obtained for the signal sample using the PMCS framework and it is summarized in Table IV.

In the third step, after the application of the response matrix, the resulting spectrum has to be corrected for events which would have passed the reconstruction level cuts but not the particle level selection, via

$$N_i^{\text{corr}} = \frac{N_i}{F_i}.$$

Here F_i is the fiducial correction factor in u_T bin i and N_i^{corr} is the number of fiducial-corrected events on the reconstruction level in bin i. The corresponding fiducial correction factors are derived from the nominal signal sample using PMCS and are summarized in Table V.

Finally, in order to get the shape of the distribution, the folded u_T distribution is normalized to unity. The fraction of the events in each u_T bin, $\mathcal{N}_i$, is calculated via the following formula:

$$\mathcal{N}_i = \frac{N_i^{\text{corr}}}{\sum_{j=1}^{5} N_j^{\text{corr}}}$$

This normalized u_T distribution is the folded result, which can be compared to the background-subtracted data directly.

This fast folding procedure is demonstrated to give reconstruction level distributions consistent with those

TABLE III. The efficiency correction $\mathcal{E}(p_T^W)$ in each p_T^W bin. The efficiency correction is the probability to pass the ion selection for the events that pass the particle level selection.

p_T^W bin	0–2 GeV	2–5 GeV	5–8 GeV	8–11 GeV	11–15 GeV	15–600 GeV
$\mathcal{E}(p_T^W)$	0.2330	0.2367	0.2387	0.2396	0.2385	0.2332

TABLE IV. Detector response matrix. The number in each cell is the probability for the events in one p_T^W bin to be reconstructed into different u_T bins.

p_T^W bin	0–2 GeV	2–5 GeV	5–8 GeV	8–11 GeV	11–15 GeV	15–600 GeV
$0 < u_T < 2$ GeV	0.1784	0.1696	0.1212	0.0745	0.0372	0.0069
$2 < u_T < 5$ GeV	0.4636	0.4588	0.4109	0.3163	0.1974	0.0452
$5 < u_T < 8$ GeV	0.2452	0.2524	0.2966	0.3331	0.3146	0.1121
$8 < u_T < 11$ GeV	0.0806	0.0863	0.1193	0.1810	0.2495	0.1637
$11 < u_T < 15$ GeV	0.0269	0.0270	0.0428	0.0775	0.1550	0.2210

TABLE V. The fiducial correction $F(u_T)$ in each u_T bin. The fiducial correction is the probability to pass the particle level selection for the events that pass the ion selection.

u_T bin	0–2 GeV	2–5 GeV	5–8 GeV	8–11 GeV	11–15 GeV
$F(u_T)$	0.8624	0.8689	0.8797	0.8812	0.9036

provided by PMCS for the models studied in this paper. Both the efficiency correction and the response matrix are applied directly to the p_T^W distribution and hence no model assumptions are made. However, the fiducial correction could depend on details of the theoretical model used. We have tested this possibility using two toy production models which differ from our baseline model by either shifting the peak in the p_T^W distribution by 20% or by broadening the peak by about 20%. In these cases, the u_T distributions resulting from the fast folding procedure differed negligibly from those using PMCS.

In order to calculate the chi-square value for the difference between the folded theory prediction and the background-subtracted data, the uncertainty of the folded distribution in each u_T bin and the bin-by-bin correlation matrix are also needed. In this fast folding procedure, the detector response is represented by two corrections, the fiducial correction and the efficiency correction, and one detector response matrix. Since the systematic uncertainty is estimated from the difference in the normalized u_T distribution between the nominal response and the systematic variation, the uncertainty and the correlation matrix are model dependent, which is why the folding inputs for all of the systematic variations must be provided.

The uncertainty on the u_T distribution consists of three independent parts: the uncertainty due to the MC statistics, the uncertainty due to the hadronic recoil calibration, and the uncertainty due to the electron identification and reconstruction efficiencies and the electron energy response. The dominant uncertainty is the one due to the hadronic recoil. The uncertainty due to the MC statistics is directly provided in Table VI, which is considered to be bin-by-bin uncorrelated.

The other two parts of the uncertainty should be estimated with systematic variations. There are eleven systematic variations provided in total, ten for the uncertainty due to the hadronic recoil calibration and one for the uncertainty due to the efficiency and the energy response of the electron. The hadronic recoil response and resolution are characterized by the five uncorrelated parameters discussed in Sec. VI. The uncertainties due to positive and negative changes in these parameters differ, so we must evaluate both signs of parameter change, thus giving the first ten variations. The eleventh systematic variation is derived with the parameter α, which is mentioned in Sec. IV, changed by its uncertainty. This is an overestimation of the uncertainty due to the strong anticorrelation between α and β. The folding inputs of these eleven systematic variations are provided in Tables VII, VIII, and IX. The uncertainties from different variations are considered to be uncorrelated and the uncertainty from each variation is considered to be bin-by-bin correlated. The bin-by-bin covariance matrix of systematic variation k is defined as $\Sigma^{(k)}$, whose element is calculated via

$$\Sigma_{ij}^{(k)} = (\mathcal{N}_i - \mathcal{N}_i^{(k)}) \times (\mathcal{N}_j - \mathcal{N}_j^{(k)}).$$

TABLE VI. The systematic uncertainty due to the MC statistics in each u_T bin of the folded result.

u_T bin	0–2 GeV	2–5 GeV	5–8 GeV	8–11 GeV	11–15 GeV
Uncertainty due to the MC statistics in the folded u_T distribution	0.0005	0.0007	0.0006	0.0005	0.0004

TABLE VII. The efficiency correction $\mathcal{E}(p_T^W)$ in each p_T^W bin from eleven systematic variations. The efficiency correction is the probability to pass the reconstruction level selection for the events that pass the particle level selection. The first ten systematic variations are for the uncertainty due to the hadronic recoil and the last one is for the uncertainty due to the electron energy response.

p_T^W bin	0–2 GeV	2–5 GeV	5–8 GeV	8–11 GeV	11–15 GeV	15–600 GeV
Systematic Variation No. 1	0.2348	0.2374	0.2377	0.2405	0.2392	0.2332
Systematic Variation No. 2	0.2345	0.2370	0.2392	0.2377	0.2382	0.2334
Systematic Variation No. 3	0.2336	0.2374	0.2388	0.2377	0.2378	0.2317
Systematic Variation No. 4	0.2335	0.2369	0.2394	0.2385	0.2379	0.2329
Systematic Variation No. 5	0.2323	0.2365	0.2392	0.2385	0.2393	0.2326
Systematic Variation No. 6	0.2337	0.2355	0.2390	0.2408	0.2387	0.2321
Systematic Variation No. 7	0.2342	0.2373	0.2384	0.2386	0.2390	0.2318
Systematic Variation No. 8	0.2328	0.2362	0.2384	0.2386	0.2390	0.2322
Systematic Variation No. 9	0.2360	0.2369	0.2382	0.2398	0.2376	0.2323
Systematic Variation No. 10	0.2327	0.2371	0.2387	0.2390	0.2387	0.2328
Systematic Variation No. 11	0.2343	0.2370	0.2379	0.2399	0.2374	0.2315

TABLE VIII.   Detector response matrices for the eleven systematic variations. The numbers in each cell are the probability for the events in one p_T^W bin to be reconstructed into different u_T bins. The first ten systematic variations are for the uncertainty due to the hadronic recoil and the last one is for the uncertainty due to the electron energy response.

p_T^W bin	0–2 GeV	2–5 GeV	5–8 GeV	8–11 GeV	11–15 GeV	15–600 GeV
			Systematic Variation No. 1			
$0 < u_T < 2$	0.1876	0.1738	0.1196	0.0715	0.0363	0.0071
$2 < u_T < 5$	0.4642	0.4588	0.4109	0.3120	0.2022	0.0456
$5 < u_T < 8$	0.2382	0.2503	0.2938	0.3388	0.3107	0.1112
$8 < u_T < 11$	0.0777	0.0840	0.1227	0.1822	0.2535	0.1644
$11 < u_T < 15$	0.0272	0.0275	0.0439	0.0780	0.1503	0.2216
			Systematic Variation No. 2			
$0 < u_T < 2$	0.1754	0.1669	0.1193	0.0720	0.0356	0.0070
$2 < u_T < 5$	0.4665	0.4607	0.4091	0.3144	0.2009	0.0457
$5 < u_T < 8$	0.2410	0.2506	0.2957	0.3323	0.3113	0.1137
$8 < u_T < 11$	0.0834	0.0880	0.1231	0.1838	0.2511	0.1667
$11 < u_T < 15$	0.0280	0.0281	0.0437	0.0788	0.1532	0.2209
			Systematic Variation No. 3			
$0 < u_T < 2$	0.1776	0.1702	0.1200	0.0698	0.0340	0.0067
$2 < u_T < 5$	0.4647	0.4618	0.4098	0.3203	0.1988	0.0442
$5 < u_T < 8$	0.2393	0.2496	0.2967	0.3359	0.3078	0.1121
$8 < u_T < 11$	0.0850	0.0852	0.1222	0.1802	0.2584	0.1630
$11 < u_T < 15$	0.0273	0.0275	0.0428	0.0762	0.1542	0.2245
			Systematic Variation No. 4			
$0 < u_T < 2$	0.1815	0.1744	0.1215	0.0730	0.0366	0.0068
$2 < u_T < 5$	0.4612	0.4577	0.4110	0.3157	0.2022	0.0467
$5 < u_T < 8$	0.2440	0.2505	0.2941	0.3311	0.3114	0.1126
$8 < u_T < 11$	0.0811	0.0842	0.1209	0.1817	0.2509	0.1641
$11 < u_T < 15$	0.0263	0.0279	0.0438	0.0799	0.1504	0.2199
			Systematic Variation No. 5			
$0 < u_T < 2$	0.1808	0.1697	0.1199	0.0707	0.0355	0.0067
$2 < u_T < 5$	0.4623	0.4617	0.4129	0.3213	0.1973	0.0443
$5 < u_T < 8$	0.2424	0.2498	0.2940	0.3354	0.3130	0.1121
$8 < u_T < 11$	0.0818	0.0857	0.1212	0.1792	0.2526	0.1676
$11 < u_T < 15$	0.0274	0.0277	0.0422	0.0760	0.1561	0.2229
			Systematic Variation No. 6			
$0 < u_T < 2$	0.1740	0.1716	0.1241	0.0739	0.0364	0.0066
$2 < u_T < 5$	0.4625	0.4609	0.4116	0.3207	0.2011	0.0462
$5 < u_T < 8$	0.2446	0.2489	0.2917	0.3303	0.3145	0.1113
$8 < u_T < 11$	0.0857	0.08433	0.1210	0.1817	0.246	0.1649
$11 < u_T < 15$	0.0280	0.0287	0.0429	0.0758	0.1537	0.2216
			Systematic Variation No. 7			
$0 < u_T < 2$	0.1803	0.1725	0.1233	0.0711	0.0352	0.0071
$2 < u_T < 5$	0.4648	0.4612	0.4121	0.3197	0.2025	0.0454
$5 < u_T < 8$	0.2423	0.2507	0.2934	0.3320	0.3110	0.1092
$8 < u_T < 11$	0.0810	0.0832	0.1188	0.1826	0.2545	0.1643
$11 < u_T < 15$	0.0263	0.0268	0.0434	0.0768	0.1493	0.2239
			Systematic Variation No. 8			
$0 < u_T < 2$	0.1805	0.1722	0.1218	0.0705	0.0379	0.0070
$2 < u_T < 5$	0.4648	0.4602	0.4123	0.3172	0.2052	0.0466
$5 < u_T < 8$	0.2399	0.2481	0.2927	0.3379	0.3114	0.1137
$8 < u_T < 11$	0.0826	0.0863	0.1215	0.1805	0.2477	0.1653
$11 < u_T < 15$	0.0266	0.0278	0.0432	0.0764	0.1517	0.2235

(Table continued)

TABLE VIII. *(Continued)*

p_T^W bin	0–2 GeV	2–5 GeV	5–8 GeV	8–11 GeV	11–15 GeV	15–600 GeV
			Systematic Variation No. 9			
$0 < u_T < 2$	0.1774	0.1709	0.1241	0.0717	0.0348	0.0064
$2 < u_T < 5$	0.4618	0.4563	0.4077	0.3188	0.1980	0.0445
$5 < u_T < 8$	0.2444	0.2525	0.2958	0.3335	0.3138	0.1116
$8 < u_T < 11$	0.0833	0.0866	0.1216	0.1798	0.2512	0.1657
$11 < u_T < 15$	0.0275	0.0278	0.0417	0.0782	0.1542	0.2226
			Systematic Variation No. 10			
$0 < u_T < 2$	0.1826	0.1720	0.1198	0.0708	0.0370	0.0073
$2 < u_T < 5$	0.4598	0.4584	0.4100	0.3168	0.2026	0.0469
$5 < u_T < 8$	0.2420	0.2483	0.2988	0.3346	0.3091	0.1120
$8 < u_T < 11$	0.0827	0.0876	0.1195	0.1819	0.2494	0.1628
$11 < u_T < 15$	0.0273	0.0278	0.0430	0.0774	0.1546	0.2204
			Systematic Variation No. 11			
$0 < u_T < 2$	0.1790	0.1707	0.1192	0.0716	0.0349	0.0072
$2 < u_T < 5$	0.4624	0.4629	0.4102	0.3176	0.2030	0.0472
$5 < u_T < 8$	0.2436	0.2484	0.2967	0.3341	0.3116	0.1108
$8 < u_T < 11$	0.0839	0.0853	0.1223	0.1830	0.2483	0.1653
$11 < u_T < 15$	0.0259	0.0271	0.0431	0.0763	0.1561	0.2229

TABLE IX. The fiducial correction $F(u_T)$ in each u_T bin for the eleven systematic variations. The fiducial correction is the probability to pass the particle level selection for the events that pass the ion selection. The first ten systematic variations are for the uncertainty due to the hadronic recoil and the last one is for the uncertainty due to the electron energy response.

u_T bin	0–2 GeV	2–5 GeV	5–8 GeV	8–11 GeV	11–15 GeV
Systematic Variation No. 1	0.8639	0.8705	0.8778	0.8814	0.9011
Systematic Variation No. 2	0.8629	0.8686	0.8787	0.8817	0.9033
Systematic Variation No. 3	0.8612	0.8703	0.8796	0.8824	0.9003
Systematic Variation No. 4	0.8637	0.8673	0.8789	0.8819	0.9002
Systematic Variation No. 5	0.8637	0.8690	0.8803	0.8795	0.9037
Systematic Variation No. 6	0.8638	0.8686	0.8779	0.8799	0.9020
Systematic Variation No. 7	0.8634	0.8691	0.8805	0.8830	0.8996
Systematic Variation No. 8	0.8651	0.8695	0.8795	0.8821	0.8992
Systematic Variation No. 9	0.8664	0.8691	0.8800	0.8819	0.9004
Systematic Variation No. 10	0.8630	0.8691	0.8786	0.8808	0.9007
Systematic Variation No. 11	0.8615	0.8700	0.8798	0.8842	0.9004

Here $\mathcal{N}_i^{(k)}$ is the folded result from systematic variation k. The covariance matrix of the uncertainty due to the hadronic recoil calibration are calculated by the average of the covariance matrices from the positive and negative changes. The covariance matrix of the total systematic uncertainty, $\Sigma^{(\mathrm{Syst})}$, is calculated as the sum of the covariance matrix of the uncertainty due to the hadronic recoil calibration and that of the uncertainty due to the efficiency and the energy response of the electron, via

$$\Sigma^{(\mathrm{Syst})} = \frac{\sum_{k=1}^{10} \Sigma^{(k)}}{2} + \Sigma^{(11)}.$$

The total uncertainty of the folded result is the combination of the statistical uncertainty and the total systematic uncertainty. The total covariance matrix used in the χ^2 calculation, $\Sigma^{(\mathrm{Total})}$, is the sum of the covariance matrix of the systematic uncertainty and the statistical uncertainties due to both data and MC statistics, $\Sigma^{(\mathrm{Data\ stat})}$ and $\Sigma^{(\mathrm{MC\ stat})}$, via

$$\Sigma^{(\mathrm{Total})} = \Sigma^{(\mathrm{Data\ stat})} + \Sigma^{(\mathrm{MC\ stat})} + \Sigma^{(\mathrm{Syst})}.$$

Here $\Sigma^{(\mathrm{Data\ stat})}$ is a diagonal matrix constructed with the total uncertainty provided in Table I and $\Sigma^{(\mathrm{MC\ stat})}$ is also a diagonal matrix constructed with the uncertainty summarized in Table VI.

As a validation, the χ^2 values calculated from the fast folding approach are compared to those provided in Table II. The background-subtracted data is fluctuated with the statistical uncertainty from the data in order to estimate the impact on χ^2/ndf from the data statistics. The difference between the chi-square values calculated from the PMCS simulation and that calculated from the fast folding is negligible compared to the impact of the statistical fluctuation of the data, hence validating this approach.

[1] M. Schott and M. Dunford, Review of single vector boson production in pp collisions at $\sqrt{s}$ = 7-TeV, Eur. Phys. J. C **74**, 2916 (2014).

[2] J. Collins, D. E. Soper, and G. Sterman, Transverse momentum distribution in Drell-Yan pair and W and Z boson production, Nucl. Phys. **B250**, 199 (1985).

[3] C. Balazs and C. P. Yuan, Soft gluon effects on lepton pairs at hadron colliders, Phys. Rev. D **56**, 5558 (1997).

[4] T. Becher and M. Neubert, Drell-Yan production at small q_T, transverse parton distributions and the collinear anomaly, Eur. Phys. J. C **71**, 1665 (2011).

[5] S. Catani *et al.*, Vector boson production at hadron colliders: Transverse-momentum resummation and leptonic decay, J. High Energy Phys. 12 (2015) 047.

[6] M. A. Ebert and F. J. Tackmann, Resummation of transverse momentum distributions in distribution space, J. High Energy Phys. 02 (2017) 110.

[7] W. Bizon, P. F. Monni, E. Re, L. Rottoli, and P. Torrielli, Momentum-space resummation for transverse observables and the Higgs $p_\perp$ at N^{3}LL + NNLO, J. High Energy Phys. 02 (2018) 108.

[8] J. Bellm *et al.*, HERWIG 7.0/HERWIG++ 3.0 release note, Eur. Phys. J. C **76**, 196 (2016).

[9] T. Sjstrand, S. Ask, J. R. Christiansen, R. Corke, N. Desai, P. Ilten, S. Mrenna, S. Prestel, C. O. Rasmussen, and P. Z. Skands, An introduction to PYTHIA 8.2, Comput. Phys. Commun. **191**, 159 (2015).

[10] E. Bothmann *et al.*, Event Generation with Sherpa 2.2, SciPost Phys. **7**, 034 (2019).

[11] G. A. Ladinsky and C. P. Yuan, The nonperturbative regime in QCD resummation for gauge boson production at hadron colliders, Phys. Rev. D **50**, R4239 (1994).

[12] A. V. Konychev and P. M. Nadolsky, Universality of the Collins-Soper-Sterman nonperturbative function in gauge boson production, Phys. Lett. B **633**, 710 (2006).

[13] V. M. Abazov *et al.* (D0 Collaboration), Measurement of the Shape of the Boson Transverse Momentum Distribution in $p\bar{p} \to Z/\gamma^* \to e^+e^- + X$ Events Produced at $\sqrt{s}$ = 1.96-TeV-TeV, Phys. Rev. Lett. **100**, 102002 (2008).

[14] V. M. Abazov *et al.* (D0 Collaboration), Measurement of the normalized $Z/\gamma^- > \mu^+\mu^-$ transverse momentum distribution in $p\bar{p}$ collisions at $\sqrt{s}$ = 1.96 TeV, Phys. Lett. B **693**, 522 (2010).

[15] V. M. Abazov *et al.* (D0 Collaboration), Precise Study of the Z/γ^* Boson Transverse Momentum Distribution in $p\bar{p}$ Collisions using a Novel Technique, Phys. Rev. Lett. **106**, 122001 (2011).

[16] T. Aaltonen *et al.* (CDF Collaboration), Transverse momentum cross section of e^+e^- pairs in the Z-boson region from $p\bar{p}$ collisions at $\sqrt{s}$ = 1.96 TeV, Phys. Rev. D **86**, 052010 (2012).

[17] G. Aad, A. N. Rozanov, M. I. Vysotsky, and E. V. Zhemchugov (ATLAS Collaboration), Measurement of the transverse momentum and ϕ_η^* distributions of DrellYan lepton pairs in protonproton collisions at $\sqrt{s}$ = 8 TeV with the ATLAS detector, Eur. Phys. J. C **76**, 1 (2016).

[18] G. Aad *et al.* (ATLAS Collaboration), Measurement of the Z/γ^* boson transverse momentum distribution in pp collisions at $\sqrt{s}$ = 7 TeV with the ATLAS detector, J. High Energy Phys. 09 (2014) 145.

[19] G. Aad *et al.* (ATLAS Collaboration), Measurement of the transverse momentum distribution of W bosons in pp collisions at $\sqrt{s}$ = 7 TeV with the ATLAS detector, Phys. Rev. D **85**, 012005 (2012).

[20] S. Chatrchyan *et al.* (CMS Collaboration), Measurement of the Z boson differential cross section in transverse momentum and rapidity in protonproton collisions at 8 TeV, Phys. Lett. B **749**, 187 (2015).

[21] S. Chatrchyan *et al.* (CMS Collaboration), Measurement of the rapidity and transverse momentum distributions of Z bosons in pp collisions at $\sqrt{s}$ = 7 TeV, Phys. Rev. D **85**, 032002 (2012).

[22] S. Chatrchyan *et al.* (CMS Collaboration), Measurement of the transverse momentum spectra of weak vector bosons produced in proton-proton collisions at $\sqrt{s}$ = 8 TeV, J. High Energy Phys. 02 (2017) 096.

[23] V. M. Abazov *et al.* (D0 Collaboration), Measurement of the Shape of the Transverse Momentum Distribution of W Bosons Produced in $p\bar{p}$ Collisions at sqrt(s)= 1.8 TeV, Phys. Rev. Lett. **80**, 5498 (1998).

[24] V. M. Abazov *et al.* (D0 Collaboration), Differential cross section for W boson production as a function of transverse momentum in proton-antiproton collisions at 1.8 TeV, Phys. Lett. B **513**, 292 (2001).

[25] G. Aad *et al.* (ATLAS Collaboration), Measurement of the transverse momentum distribution of W bosons in pp collisions at $\sqrt{(s)}$ = 7 TeV with the ATLAS detector, Phys. Rev. D **85**, 012005 (2012).

[26] V. M. Abazov *et al.* (D0 Collaboration), Measurement of the W Boson Mass with the D0 Detector, Phys. Rev. Lett. **108**, 151804 (2012).

[27] V. M. Abazov *et al.* (D0 Collaboration), The upgraded D0 detector, Nucl. Instrum. Methods Phys. Res., Sect. A **565**, 463 (2006).

[28] V. M. Abazov *et al.* (D0 Collaboration), Measurement of the *W* boson mass with the D0 detector, Phys. Rev. D **89,** 012005 (2014).

[29] P. Golonka and Z. Was, PHOTOS Monte Carlo: A precision tool for QED corrections in *Z* and *W* decays, Eur. Phys. J. C **45,** 97 (2006).

[30] F. Landry, R. Brock, P. M. Nadolsky, and C.-P. Yuan, Tevatron Run-1 *Z* boson data and Collins-Soper-Sterman resummation formalism, Phys. Rev. D **67,** 073016 (2003).

[31] P. M. Nadolsky, H.-L. Lai, Q.-H. Cao, J. Huston, J. Pumplin, D. Stump, W.-K. Tung, and C.-P. Yuan, Implications of CTEQ global analysis for collider observables, Phys. Rev. D **78,** 013004 (2008).

[32] T. J. Hou *et al.*, CT14 intrinsic charm parton distribution functions from CTEQ-TEA global analysis, J. High Energy Phys. 1802 (2018) 059.

[33] S. Dulat, T.-J. Hou, J. Gao, M. Guzzi, J. Huston, P. Nadolsky, J. Pumplin, C. Schmidt, D. Stump, and C.-P. Yuan, New parton distribution functions from a global analysis of quantum chromodynamics, Phys. Rev. D **93,** 033006 (2016).

[34] J. Pumplin, D. R. Stump, J. Huston, H.-L. Lai, P. Nadolsky, and W.-K. Tung, New generation of parton distributions with uncertainties from global QCD analysis, J. High Energy Phys. 07 (2002) 012.

[35] A. D. Martin, W. J. Stirling, R. S. Thorne, and G. Watt, Parton distributions for the LHC, Eur. Phys. J. C **63,** 189 (2009).

[36] A. D. Martin, W. J. Stirling, and R. S. Thorne, MRST partons generated in a fixed-flavor scheme, Phys. Lett. B **636,** 259 (2006).

[37] P. Sun, J. Isaacson, C.-P. Yuan, and F. Yuan, Nonperturbative functions for SIDIS and Drell-Yan processes, Int. J. Mod. Phys. A **33,** 1841006 (2018).

[38] G. Aad *et al.* (ATLAS Collaboration), Summary of ATLAS PYTHIA 8 tunes, Report No. ATL-PHYS-PUB-2012-003, CERN.

[39] R. Corke and T. Sjstrand, Interleaved parton showers and tuning prospects, J. High Energy Phys. 03 (2011) 032.

[40] S. Chatrchyan *et al.* (CMS Collaboration), Event generator tunes obtained from underlying event and multiparton scattering measurements, Eur. Phys. J. C **76,** 155 (2016).

[41] R. Brun and F. Carminati, CERN Program Library Long Writeup W5013, 1993 (to be published).

[42] J. Alitti *et al.* (UA2 Collaboration), An improved determination of the ratio of *W* and *Z* masses at the CERN $\bar{p}p$ collider, Phys. Lett. B **276,** 354 (1992).